






Calculation of nuclear matrix elements for $0\nu\beta\beta$ decay of ^{124}Sn using the nonclosure approach in the nuclear shell model

Shahariar Sarkar ^{1,*}, P. K. Rath,² V. Nanal ³, R. G. Pillay ¹, Pushpendra P. Singh ¹, Y. Iwata,⁴
K. Jha ¹ and P. K. Raina^{1,†}

¹Department of Physics, Indian Institute of Technology Ropar, Rupnagar 140001, Punjab, India

²Department of Physics, University of Lucknow, Lucknow 226007, India

³Department of Nuclear and Atomic Physics, Tata Institute of Fundamental Research, Mumbai 400005, India

⁴Faculty of International Studies, Osaka University of Economics and Law, Yao, Osaka 581-0853, Japan



(Received 17 August 2023; accepted 22 December 2023; published 1 February 2024)

In this study, we calculate the nuclear matrix elements (NMEs) for the light neutrino-exchange mechanism of neutrinoless double beta decay ($0\nu\beta\beta$) of ^{124}Sn within the framework of the interacting nuclear shell model, using the effective shell model Hamiltonian GCN5082. The NMEs are calculated employing both closure and nonclosure approaches. For the intermediate nucleus ^{124}Sb , effects of energy of 100 states for each $J_k^\pi = 0^+$ to 11^+ and 2^- to 9^- ($\Delta J_k = 1$) are explicitly included in the nonclosure approach. The optimal closure energy, which reproduces nonclosure NMEs using the closure approach, is found to be ≈ 3 MeV for $0\nu\beta\beta$ decay of ^{124}Sn . The NMEs for $0\nu\beta\beta$ decay of ^{124}Sn did not fully converge with 100 intermediate states for each spin-parity of ^{124}Sb . A comparison of NMEs and lower limits of $T_{1/2}^{0\nu}$ with some of the recent calculations is presented. Further, to gain a comprehensive understanding of the role of nuclear structure on the $0\nu\beta\beta$ decay, the dependence of NMEs on the spin-parity of the intermediate states, coupled spin-parity of neutrons and protons, and the number of intermediate states, is explored. The estimated lower limit on the half-life $T_{1/2}^{0\nu} \approx 7.49 \times 10^{26}$ yr provides valuable input for the experimental investigations of $0\nu\beta\beta$ decay of ^{124}Sn in India and elsewhere.

DOI: [10.1103/PhysRevC.109.024301](https://doi.org/10.1103/PhysRevC.109.024301)

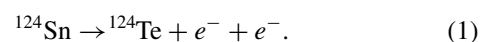
I. INTRODUCTION

The $0\nu\beta\beta$ decay is a rare weak nuclear decay that can occur in certain even-even nuclei. During this process, two neutrons inside the nucleus are converted into two protons and two electrons without emitting any neutrinos. This phenomenon violates the lepton number conservation, and a neutrino is involved as a virtual intermediate particle [1–4]. Observation of this rare decay process would provide strong evidence that neutrinos are Majorana particles. The Majorana nature of neutrinos is a widely favored for the explanation of the smallness of neutrino mass in many theoretical particle physics models. Also, the absolute mass scale of neutrinos is not yet known, and currently, only an upper limit has been derived. The $0\nu\beta\beta$ process is also expected to provide information on the absolute mass scale of neutrinos. The current best upper limit on the effective Majorana neutrino mass $\langle m_{\beta\beta} \rangle$, extracted from the measured $T_{1/2}^{0\nu}(^{136}\text{Xe}) \geq 2.3 \times 10^{26}$ yr using quasiparticle random phase approximation nuclear matrix element (NME), is 156 meV [5]. Whereas the predicted upper limit of m_ν from the tritium β decay experiment KATRIN is 0.8 eV [6].

Several decay mechanisms have been proposed for the $0\nu\beta\beta$ decay process [3]. The decay rate for all $0\nu\beta\beta$ decay mechanisms is related to NMEs and the absolute mass of the neutrino. These NMEs are typically calculated using theoretical nuclear many-body models [4]. Some of the widely used models are the quasiparticle random phase approximation (QRPA) [7], the interacting shell-model (ISM) [8–11], the interacting boson model (IBM) [12,13], the generator coordinate method (GCM) [14–16], the energy density functional (EDF) theory [14,15], the relativistic energy density functional (REDF) theory [15,16], and the projected Hartree-Fock Bogoliubov model (PHFB) [17]. Recently, some *ab initio* calculations of NMEs have been performed for the $0\nu\beta\beta$ decay of the lower mass nuclei ($A = 6$ –12) using the variational Monte Carlo (VMC) technique [18–20].

In India, the efforts have been initiated for the TIN.TIN experiment (The INdia's TIN detector) to search for $0\nu\beta\beta$ decay in ^{124}Sn [21], at the proposed underground facility of India-based Neutrino Observatory (INO) [22]. This motivates us to improve the reliability of NMEs for the $0\nu\beta\beta$ decay of ^{124}Sn using the nuclear shell model, which will aid in optimizing the experiment setup and extracting the absolute neutrino mass. In the present work, we focus on the simplest and standard light neutrino-exchange mechanism.

The $0\nu\beta\beta$ decay of ^{124}Sn occurs as



*Present address: Department of Physics, Indian Institute of Technology Roorkee, Roorkee - 247667, Uttarakhand, India; shahariar.sarkar@iitrr.ac.in

†pkraina@iitrr.ac.in

Previously, the NMEs for the light neutrino-exchange mechanism of $0\nu\beta\beta$ decay for ^{124}Sn was calculated using closure approximation in the nuclear shell model in Refs. [8,9,23–27]. In the closure approximation, the effects of excitation energy of all the virtual intermediate states of the $0\nu\beta\beta$ decay were approximated with constant closure energy, thereby avoiding the complexity of calculating a large number of intermediate states, which can be computationally challenging for nuclear shell model, particularly for higher mass isotopes such as ^{124}Sn . The difficult part of closure approximation is picking the correct closure energy which has no definite method yet and can greatly influence the accuracy of NMEs.

In recent years, the nonclosure approach has gained popularity due to increasing computational resources. This approach truly includes the real effects of many allowed excitation energy states for each spin-parity of the intermediate nucleus. This way we can improve the reliability of NMEs for $0\nu\beta\beta$ decay and avoid the problem of picking the correct closure energy value. This approach was first applied in the nuclear shell model calculations for $0\nu\beta\beta$ decay for ^{48}Ca [28]. Subsequently, it was also used for ^{76}Ge [29,30], ^{82}Se [31], and ^{48}Ca [32,33].

Although the nonclosure approach has been extensively used for lower mass region nuclei, it has not been applied for $0\nu\beta\beta$ decay candidates like ^{124}Sn in the higher mass region. The present study employs the nonclosure approach to calculate the NMEs of ^{124}Sn using the nuclear shell model, with an aim of examining the effects of excitation energy on a large number of intermediate states.

This paper is organized as follows. Section II outlines the theoretical formalism for computing the NMEs for $0\nu\beta\beta$ decay, and presents the expression for the decay rate. In Sec. III, we describe the nonclosure approach to NMEs calculation, which is the method employed in this study. Section IV presents the results of our calculations and provides a discussion of the findings, including a comparison to previous studies. Finally, in Sec. V, we summarize the main conclusions of our work.

II. THEORETICAL FORMALISM OF $0\nu\beta\beta$ DECAY RATE AND NME

The decay rate for the light neutrino-exchange mechanism of $0\nu\beta\beta$ decay can be written as [34]

$$[T_{\frac{1}{2}}^{0\nu}]^{-1} = G^{0\nu} g_A^4 |M^{0\nu}|^2 \left(\frac{\langle m_{\beta\beta} \rangle}{m_e} \right)^2, \quad (2)$$

where $G^{0\nu}$ is the well-known phase-space factor that can be calculated accurately [35], $M^{0\nu}$ is the total nuclear matrix element for the light neutrino-exchange mechanism, and $\langle m_{\beta\beta} \rangle$ is defined by the neutrino mass eigenvalues m_k and the neutrino mixing matrix elements U_{ek} , given in Eq. (3) of Ref. [32].

The total nuclear matrix element $M^{0\nu}$ can be expressed as the sum of Gamow-Teller (M_{GT}), Fermi (M_F), and tensor (M_T) matrix elements, as given by [34]

$$M^{0\nu} = M_{GT} - \left(\frac{g_V}{g_A} \right)^2 M_F + M_T, \quad (3)$$

where g_V and g_A are the vector and axial-vector constants, respectively. In the present work, $g_V = 1$ and the bare value of $g_A = 1.27$ is used. The matrix elements M_{GT} , M_F , and M_T of the scalar two-body transition operator O_{12}^α of $0\nu\beta\beta$ decay can be expressed as [10]

$$M_\alpha = \langle f | O_{12}^\alpha | i \rangle, \quad (4)$$

where $\alpha \in F, GT, T$, and in the present case, $|i\rangle$ corresponds to the 0^+ ground state of the parent nucleus ^{124}Sn , and $|f\rangle$ corresponds to the 0^+ ground state of the granddaughter nucleus ^{124}Te .

The calculation of two-body matrix elements (TBMEs) for $0\nu\beta\beta$ decay involves scalar two-particle transition operators O_{12}^α that incorporate both spin and radial neutrino potential operators. These operators are given by [28]

$$\begin{aligned} O_{12}^{GT} &= \tau_1 - \tau_2 - (\sigma_1 \cdot \sigma_2) H_{GT}(r, E_k), \\ O_{12}^F &= \tau_1 - \tau_2 - H_F(r, E_k), \\ O_{12}^T &= \tau_1 - \tau_2 - S_{12} H_T(r, E_k), \end{aligned} \quad (5)$$

where τ is isospin annihilation operator, $\mathbf{r} = \mathbf{r}_1 - \mathbf{r}_2$ is the internucleon distance of the decaying nucleons, and $r = |\mathbf{r}|$. The operator S_{12} is defined as $S_{12} = 3(\sigma_1 \cdot \hat{\mathbf{r}})(\sigma_2 \cdot \hat{\mathbf{r}}) - (\sigma_1 \cdot \sigma_2)$. For the light-neutrino exchange mechanism of $0\nu\beta\beta$ decay, the radial neutrino potential with explicit dependence on the energy of the intermediate states is given by [28]

$$H_\alpha(r, E_k) = \frac{2R}{\pi} \int_0^\infty \frac{f_\alpha(q, r) q dq}{q + E_k - (E_i + E_f)/2}, \quad (6)$$

where R is the radius of the parent nucleus, q is the momentum of the virtual Majorana neutrino, E_i , E_k , and E_f are the energies of initial, intermediate, and final nuclei, respectively. The $f_\alpha(q, r) = j_p(q, r) h_\alpha(q^2)$, where $j_p(q, r)$ is spherical Bessel function ($p = 0$ for Fermi and GT, and $p = 2$ for tensor NMEs). The $h_\alpha(q^2)$ accounts for the effects of finite nucleon size (FNS) and higher-order currents (HOC) which are given in Refs. [34,36]. In the expression of $h_\alpha(q^2)$, the parameters M_V and M_A are 850 MeV and 1086 MeV, respectively, while $\mu_p - \mu_n$ is 4.7 is used in the calculation [37].

In the calculation of the NMEs for $0\nu\beta\beta$ decay, it is also necessary to take into account the effects of short-range correlations (SRC). A standard method to include SRC is via a phenomenological Jastrow-like function [36,38]. By including the SRC effect in the Jastrow approach, one can write the NMEs of $0\nu\beta\beta$ defined in Eq. (4) as [36]

$$M_\alpha^{0\nu} = \langle f | f_{\text{Jastrow}}(r) O_{12}^\alpha f_{\text{Jastrow}}(r) | i \rangle, \quad (7)$$

where the Jastrow-type SRC function is defined as

$$f_{\text{Jastrow}}(r) = 1 - ce^{-ar^2} (1 - br^2). \quad (8)$$

In literature, three different SRC parametrizations are used: Miller-Spencer, charge-dependent Bonn (CD-Bonn), and Argonne V18 (AV18) to parametrize a , b , and c [37]. The parameters a , b , and c in different SRC parametrizations are given in Table I. This approach of using the Jastrow-like function to include the effects of SRC is extensively used in Refs. [27,37,39]. The authors of Refs. [40,41] have recently proposed another method namely, the unitary correlation operator method (UCOM) to estimate the effects of SRC. The

TABLE I. Parameters for the short-range correlation (SRC) parametrization of Eq. (8).

SRC type	a	b	c
Miller-Spencer	1.10	0.68	1.00
CD-Bonn	1.52	1.88	0.46
AV18	1.59	1.45	0.92

present study focuses only on the Jastrow-type approach to estimate the effects of SRC. The detailed descriptions of incorporating the SRC effects in different approaches can be found in Refs. [36,38].

III. THE NONCLOSURE APPROACH OF NME CALCULATIONS

In the nonclosure approach, the neutrino potential of Eq. (6) is computed explicitly by considering energy E_k of a large number of states $|k\rangle$ of the virtual intermediate nucleus which is ^{124}Sb for the present case. The term $E_k - (E_i + E_f)/2$ in the denominator of the neutrino potential of Eq. (6) is written as a function of excitation energy (E_k^*) of the intermediate state ($|k\rangle$) as $E_k - (E_i + E_f)/2 \rightarrow Q_{\beta\beta}(0^+)/2 + \Delta M + E_k^*$ [28], where $Q_{\beta\beta}(0^+)$ is the Q value corresponding to the $0\nu\beta\beta$ decay of ^{124}Sn , and ΔM is the

mass difference between the ^{124}Sb and ^{124}Sn isotopes and E_k^* is the excitation energy of the intermediate states $|k\rangle$ with different allowed spin-parities of ^{124}Sb .

If one approximates the term $E_k - (E_i + E_f)/2$ in the denominator of the neutrino potential of Eq. (6) with a constant closure energy ($\langle E \rangle$) value such that $E_k - (E_i + E_f)/2 \rightarrow \langle E \rangle$, it is known as closure approximation [37]. The closure approximation is widely used in the past because it eliminates the complexity of calculating a large number of virtual intermediate states, which can be computationally challenging, particularly for higher mass region isotopes using the nuclear shell model. The difficult part of closure approximation is picking the right value of constant closure energy $\langle E \rangle$ which greatly influences the accuracy of the calculated NMEs. In this paper, we focus on using the nonclosure approach to include the real effects of at least 100 states for each spin-parity of the virtual intermediate nucleus ^{124}Sb . The NMEs with the closure method are also calculated with the closure energy near the optimal value for which NMEs in closure and nonclosure methods overlap.

The method based on the nonclosure approach is known as the running nonclosure method [28] as we can only calculate a finite number of intermediate states out of all possibilities with the current computational limit. The partial NMEs for the transition operator of Eq. (5) in the running nonclosure method is defined as [33]

$$M_\alpha(J_k, J, E_k^*) = \sum_{k'_1 k'_2 k_1 k_2} \sqrt{(2J_k + 1)(2J_k + 1)(2J + 1)} (-1)^{j_{k_1} + j_{k_2} + J} \begin{Bmatrix} j_{k_1'} & j_{k_1} & J_k \\ j_{k_2} & j_{k_2'} & J \end{Bmatrix} \text{OBTD}(k, f, k'_2, k_2, J_k) \\ \times \text{OBTD}(k, i, k'_1, k_1, J_k) \langle k'_1, k'_2 : J || O_{12}^\alpha || k_1, k_2 : J \rangle. \quad (9)$$

Here, k_1 represents a set of spherical quantum numbers (n_1, l_1, j_1) for an orbital, similarly for k_2, k'_1 , and k'_2 . In the present study, k_1 (and others) has the spherical quantum numbers for $0g_{9/2}, 1d_{5/2}, 1d_{3/2}, 2s_{1/2}$, and $0h_{11/2}$ orbits for jj55 model space. The J is the allowed spin-parity of the two decaying neutrons and created protons and J_k is the allowed spin-parity of the intermediate states $|k\rangle$. The complete expression of non-anti-symmetric reduced TBME ($\langle k'_1, k'_2 : J || O_{12}^\alpha || k_1, k_2 : J \rangle$) for running nonclosure method is given in Ref. [28]. The one-body transition densities (OBTD) are the matrix elements of neutron annihilation and proton creation operators which in the proton-neutron formalism is given in Eq. (41) of Ref. [33]. Finally, in the running nonclosure method, the NMEs are calculated by summing over all intermediate states $|k\rangle$ with excitation energies E_k^* up to a certain cutoff value E_c as $M_\alpha(E_c) = \sum_{J_k, J, E_k^* \leq E_c} M_\alpha(J_k, J, E_k^*)$ [28]. The choice of the cutoff energy E_c is important, as it affects the convergence and accuracy of the calculation. Typically, the NMEs are found to be almost constant for values of E_c large enough to include all relevant intermediate states.

IV. RESULTS AND DISCUSSION

The nuclear shell model diagonalization is performed using shell model code KSHELL [46] to calculate the necessary

wave functions and energies of the initial, intermediate, and final nuclei of $0\nu\beta\beta$ decay of ^{124}Sn . The calculated wave functions are further used to calculate the OBTD that appears in the expression of NME for $0\nu\beta\beta$ decay. The shell model Hamiltonian GCN5082 [47] of jj55 model space is used as an input in the calculations. The GCN5082 was also used in the shell model calculations of Ref. [27]. Another important Hamiltonian of jj55 model space is singular value decomposition (SVD) which is used in shell model calculations of Ref. [9]. The SVD Hamiltonian is not publicly available at the time of our calculations, so we are not able to use it in our calculations. For each allowed spin-parity J_k^π of the virtual intermediate state ^{124}Sb in the $0\nu\beta\beta$ decay of ^{124}Sn , we consider the first 100 states. We then calculate the non-anti-symmetric reduced TBMEs for the running nonclosure method using a program that we have written.

Table II shows the different types of calculated NMEs for $0\nu\beta\beta$ decay of ^{124}Sn using the nonclosure method in the nuclear shell model. The corresponding results for NMEs in the closure method with closure energy $\langle E \rangle = 3.0$ MeV which is near the optimal value (as discussed later) are also given for comparison. The effects of FNS and HOC are included in all of these NMEs. In addition, results of NMEs for three different parametrizations of SRC (Miller-Spencer, CD-Bonn,

TABLE II. Nuclear matrix elements M_F , M_{GT} , M_T , and M_ν for $0\nu\beta\beta$ decay of ^{124}Sn , calculated with GCN5082 interaction using running nonclosure and running closure methods for different SRC parametrizations. The closure energy $\langle E \rangle = 3.0$ MeV is used for closure NMEs, which is near to the optimal value as discussed later.

NME type	SRC type	Nonclosure NME	Closure NME
M_F	None	-0.529	-0.529
M_F	Miller-Spencer	-0.369	-0.369
M_F	CD-Bonn	-0.564	-0.565
M_F	AV18	-0.520	-0.520
M_{GT}	None	1.961	1.954
M_{GT}	Miller-Spencer	1.414	1.410
M_{GT}	CD-Bonn	2.012	2.008
M_{GT}	AV18	1.860	1.854
M_T	None	0.016	0.015
M_T	Miller-Spencer	0.015	0.014
M_T	CD-Bonn	0.015	0.014
M_T	AV18	0.015	0.014
$M^{0\nu}$	None	2.304	2.297
$M^{0\nu}$	Miller-Spencer	1.658	1.654
$M^{0\nu}$	CD-Bonn	2.377	2.372
$M^{0\nu}$	AV18	2.198	2.192

and AV18) are also given. It is observed that the GT-type NMEs dominate over the Fermi and tensor-type NMEs, and there is a significant difference in the NMEs depending on the type of SRC used. The SRC type: none represents the case where only the effects of FNS and HOC are considered. For Miller-Spencer type SRC, the impact of SRC is most prominent. We see no significant difference in NMEs for closure and nonclosure methods as the closure energy $\langle E \rangle = 3.0$ MeV is used which is near the optimal value for which nonclosure and closure NME overlaps. In the latter part of the discussion, we will describe the method to find the exact optimal closure energy for which closure and nonclosure NMEs overlap.

In Table III, we show the total NME, calculated with ISM in nonclosure approximation for CD-Bonn SRC and the $T_{1/2}^{0\nu}$

(lower limit) of $0\nu\beta\beta$ decay of ^{124}Sn for the light neutrino-exchange mechanism along with the reported results of NMEs and $T_{1/2}^{0\nu}$ (lower limits) with different many-body nuclear models, SRC, and approximation. The NMEs are found to vary in the range of 2.15–5.30. In Ref. [9], the total NME ($M^{0\nu}$) for the CD-Bonn type of SRC was calculated to be 2.17 with closure energy of 3.5 MeV using the shell model, whereas the NME was reported to be 2.62 in Ref. [27], which was calculated in the shell model with UCOM SRC in closure approximation. The calculated $M^{0\nu}$ is 2.38 in the present study using the shell model in nonclosure approach for CD-Bonn SRC, which is about 10% larger as compared to the results of Ref. [9] and about 10% smaller as compared to the results of Ref. [27]. These differences may arise from the choice of Hamiltonian, and closure energy used in the calculations of earlier studies. The NMEs calculated with other nuclear models than the shell model are larger and it's still an open quest to minimize the gaps of this large difference of NMEs in different models.

With the calculated NMEs and considering the upper limit of $\langle m_{\beta\beta} \rangle$ of 50 meV, the lower limit of $T_{1/2}^{0\nu}$ (the light neutrino-exchange mechanism) of ^{124}Sn is predicted to be 7.49×10^{26} yr. The limit of $\langle m_{\beta\beta} \rangle \sim 50$ meV is discussed in detail in Ref. [5] and also in Refs. [48–50]. The future $0\nu\beta\beta$ decay experiments for various isotopes, including ^{124}Sn , will need a sensitivity better than 50 meV to probe the Majorana nature of neutrinos in the inverted mass ordering (IO) region, extending beyond the quasidegenerate mass region. Therefore, in the present study, the lower limit of $T_{1/2}^{0\nu}$ (^{124}Sn) has been estimated using the upper limit of $\langle m_{\beta\beta} \rangle$ as 50 meV.

A. Dependence of NMEs on spin-parity (J_k^T) of the intermediate states of ^{124}Sb

To study the contribution of each allowed spin-parity state of the virtual intermediate nucleus ^{124}Sb on the NMEs, we use

TABLE III. A comparison of NMEs (the light neutrino-exchange mechanism) and lower limits of $T_{1/2}^{0\nu}$ (^{124}Sn) calculated with different many-body nuclear models. The phase space factor $G^{0\nu} = 9.06 \times 10^{-15} (\text{yr}^{-1})$ is used in the current study which is taken from Ref. [42]. Also, considering the upper limit of 50 meV for $\langle m_{\beta\beta} \rangle$ from the inverted ordering (IO) band of neutrino mass from Fig. 3 of Ref. [5], $|\eta_{\nu L}| = \frac{\langle m_{\beta\beta} \rangle}{m_e} \approx 10^{-7}$ is used. The lower limits of $T_{1/2}^{0\nu}$ for other references are recalculated with the phase space factor and $|\eta_{\nu L}|$ of the present study, but with the respective NME and g_A quoted in those references.

Nuclear model	Reference	Approximation	g_A	SRC type	NME ($M^{0\nu}$)	$T_{1/2}^{0\nu}$ (yr) (lower limit)
ISM	Current study	Nonclosure	1.270	CD-Bonn	2.38	7.49×10^{26}
ISM	Ref. [9]	Closure	1.270	CD-Bonn	2.17	9.01×10^{26}
ISM	Ref. [27]	Closure	1.250	UCOM	2.62	6.59×10^{26}
GCM	Ref. [24]	Closure	1.254	CD-Bonn	2.76	5.86×10^{26}
IBM-2	Ref. [43]	Closure	1.269	AV18	3.19	4.18×10^{26}
QRPA	Ref. [44]	Closure	1.260	CD-Bonn	5.30	1.56×10^{26}
QRPA	Ref. [45]	Closure	1.269	AV18	2.56	6.49×10^{26}
QRPA	Ref. [45]	Closure	1.269	CD-Bonn	2.91	5.03×10^{26}
EDF	Ref. [14]	Closure	1.250	UCOM	4.81	1.95×10^{26}
REDF	Ref. [16]	Closure	1.254	None	4.33	2.38×10^{26}

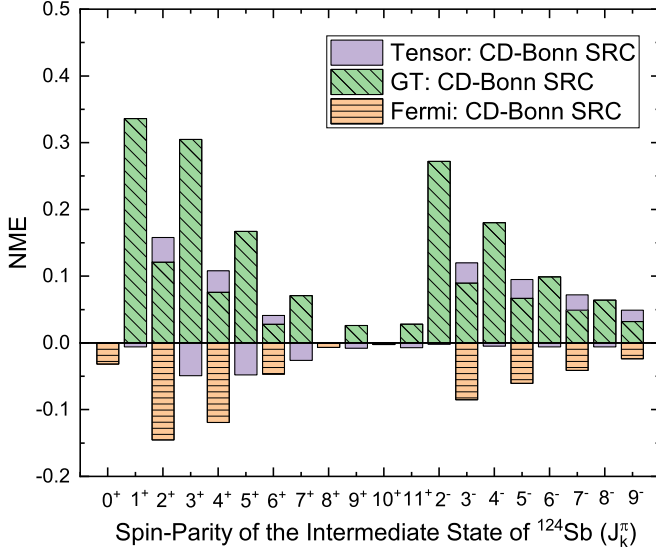


FIG. 1. The figure shows the contribution through different spin-parity of virtual intermediate states of ^{124}Sb (J_k^π) in NMEs for the light neutrino-exchange mechanism of $0\nu\beta\beta$ decay of ^{124}Sn . The NMEs are calculated using the running nonclosure method with GCN5082 effective interaction and CD-Bonn SRC parametrization.

the expression of Eq. (9) and calculate the partial NMEs as

$$M_\alpha(E_c, J_k) = \sum_{J, E_k^* \leq E_c} M_\alpha(J_k, J, E_k^*). \quad (10)$$

Here, J_k^π represents the spin-parity state of the intermediate nucleus ^{124}Sb . Figure 1 shows the dependence of the different types of NMEs on the spin-parity states of ^{124}Sb . We find that for all Fermi-type NMEs, the contribution through each J_k^π is negative, whereas, for all Gamow-Teller-type NMEs, the contribution is positive. In the case of tensor NMEs, the contributions from different J_k^π states come in the opposite phase, reducing the total tensor NMEs.

We observe that the most dominant contribution to M_F type NMEs comes from the 2^+ state, with significant contributions from 4^+ , 6^+ , 3^- , 5^- , and 7^- states. For M_{GT} type NMEs, all J_k^π contribute significantly, except for the 0^+ state. The most dominant contributions come through 1^+ state. For M_T type NMEs, prominent negative contributions come from 3^+ , 5^+ , and 7^+ states, with the contributions from 3^+ state being the most dominant. Contributions from 2^+ , 4^+ , 6^+ , 3^- , 5^- , 7^- , and 9^- states are all positive. We observe a similar pattern of variation of different types of NMEs with J_k^π for other types of SRC parametrization as well.

B. Dependence of NMEs on coupled spin-parity (J^π) of two decaying neutrons and two created protons

We have also analyzed the dependence of NMEs on the coupled spin-parity (J^π) of the two decaying neutrons and two created protons in the decay. To do this, we use the running nonclosure method with the CD-Bonn SRC parametrization

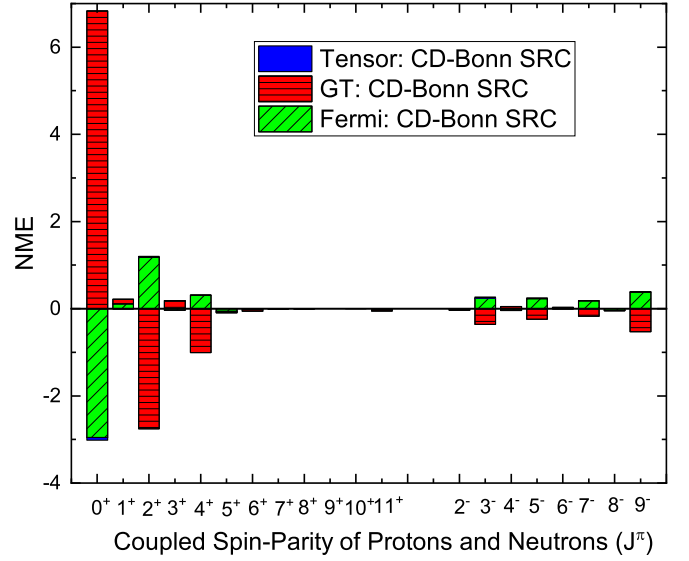


FIG. 2. Contribution through different coupled spin-parity of two initial neutrons or two final created protons (J^π) in NMEs for the light neutrino-exchange mechanism of $0\nu\beta\beta$ decay of ^{124}Sn . The results show NMEs calculated in running the nonclosure method with GCN5082 effective interaction for CD-Bonn SRC parametrization.

and write the NMEs as

$$M_\alpha(E_c, J) = \sum_{J_k, E_k^* \leq E_c} M_\alpha(J_k, J, E_k^*). \quad (11)$$

The contributions of NMEs through different J^π are shown in Fig. 2. We observe that for all types of NMEs, the most dominant contributions come from the 0^+ and 2^+ states. Additionally, the contribution from 0^+ and 2^+ states have opposite signs, leading to a reduction in the total NMEs. There are also small contributions from the 4^+ and 6^+ states, with almost negligible contributions from odd- J^π states. This is due to the pairing effect, which is responsible for the dominance of even- J^π contributions [10].

C. Variation of NMEs for $0\nu\beta\beta$ with the cutoff number of states (N_c) of ^{124}Sb

To assess the impact of the number of states on the calculated NMEs, we examine the dependence of the NMEs on the N_c for each allowed J_k^π of ^{124}Sb . We express the NMEs as a function of N_c in the running nonclosure method as

$$M_\alpha(N_c) = \sum_{J_k, J, N_k \leq N_c} M_\alpha(J_k, J, N_k), \quad (12)$$

where $M_\alpha(J_k, J, N_k)$ is the same as defined in Eq. (9).

The dependence of the different types of NMEs on the cutoff number of excitation energy states (N_c) of ^{124}Sb is shown in Fig. 3 in both closure and nonclosure methods. In the present study, we were able to consider $N_c = 100$ for each allowed J_k^π of ^{124}Sb with our available computational facility. It is observed that even with 100 intermediate states for each spin-parity of ^{124}Sb , the NMEs for $0\nu\beta\beta$ decay of ^{124}Sn in

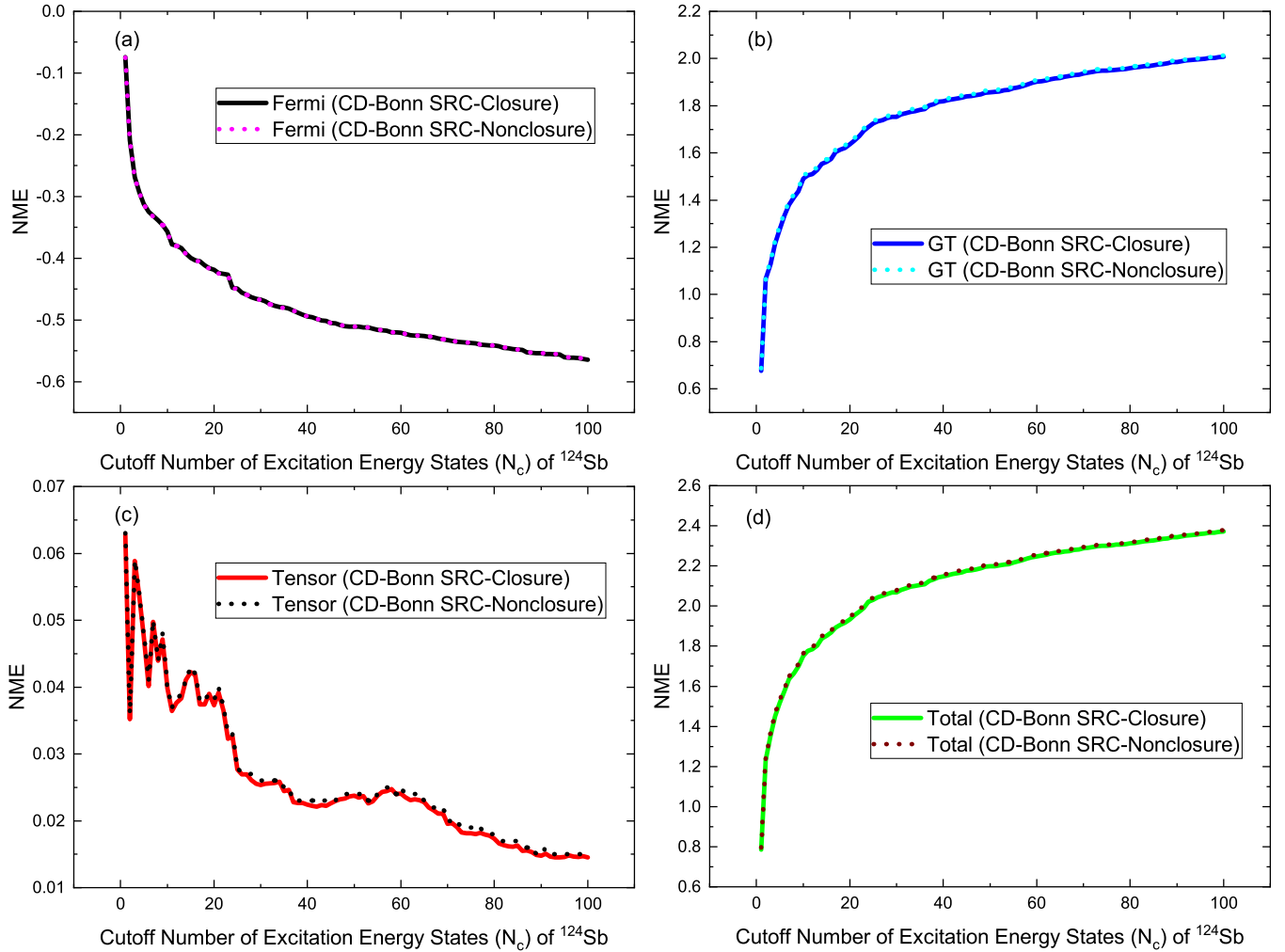


FIG. 3. The figure shows the variation of (a) Fermi, (b) Gamow-Teller, (c) tensor, and (d) total NMEs for the $0\nu\beta\beta$ (the light neutrino-exchange mechanism) of ^{124}Sn with the cutoff number of excitation energy states (N_c) of the virtual intermediate nucleus ^{124}Sb . The NMEs are calculated using the total GCN5082 interaction for the CD-Bonn short-range correlation (SRC) parametrization in the running nonclosure (dotted lines) and closure (solid lines) methods. The optimal value of the closure energy $\langle E \rangle \approx 3.0$ MeV is used for closure NMEs (see text for details).

both closure and nonclosure methods did not exhibit full convergence. However, the NME approaches near convergence as the number of states increases. While the values of the tensor-type NMEs are not yet saturated even at $N_c = 100$, this is not a problem as the contribution from tensor-type NMEs is negligible compared to the GT and Fermi-type NMEs. We note that a similar dependence of NMEs on N_c is seen for other SRC parametrizations.

It is crucial to emphasize that employing an optimal closure energy value of $\langle E \rangle \approx 3$ MeV reproduced the nonclosure NMEs utilizing the closure method, across all cutoff number of states for each spin-parity of the intermediate nucleus ^{124}Sb . It is expected that the trend of NME dependence on the cutoff number of states for ^{124}Sb , in both closure and nonclosure methodologies, may persist beyond 100 intermediate states for each spin-parity of ^{124}Sb . This further emphasizes the effectiveness of the extracted optimal closure energy in reproducing nonclosure NMEs using the closure approach, even when employing

a larger number of states for each spin-parity of ^{124}Sb to achieve superior convergence. This is one of the important findings of this study.

D. Finding the optimal value of closure energy for $0\nu\beta\beta$ decay of ^{124}Sn

Here, we discuss the important issue of identifying the optimal closure energy for which the NMEs in the closure and nonclosure approaches overlap. In order to accomplish this, we plot variations of Fermi, GT, tensor, and total NMEs calculated using the closure approach for different SRC parametrization with closure energy as shown in Fig. 4. The nonclosure NMEs are also shown in Fig. 4. At the optimal value of closure energy, there is a crossing of the nonclosure and closure NMEs as indicated by a vertical magenta line in Fig. 4.

The optimal closure energy for Fermi-type NMEs is determined to be around 3.1 MeV for various SRC

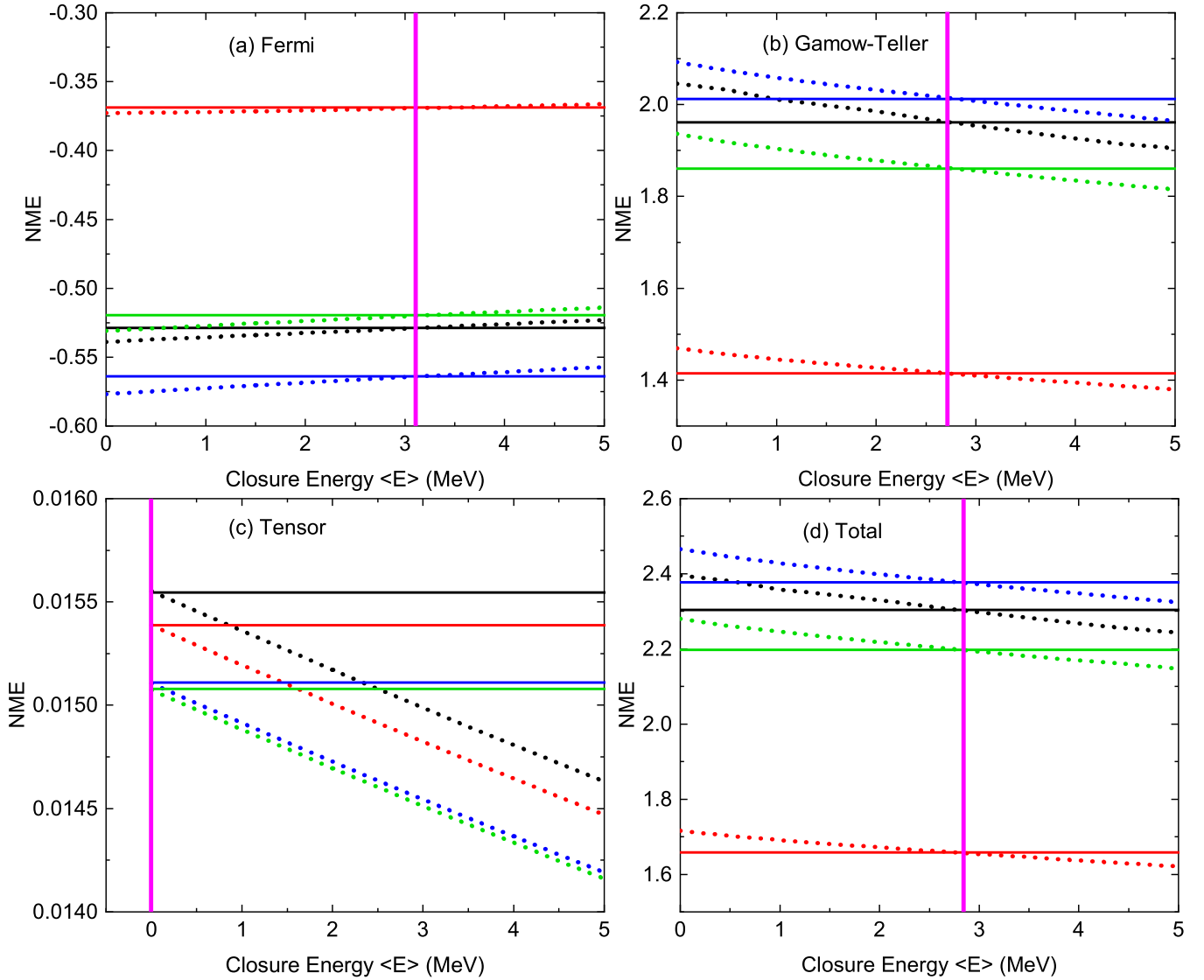


FIG. 4. The figure shows the dependence of closure NMEs of (a) Fermi, (b) Gamow-Teller, (c) tensor, and (d) total types with closure energy $\langle E \rangle$ for different SRC parametrizations. The plot also shows the nonclosure NMEs to find the crossover of closure and nonclosure NMEs (marked with a vertical magenta line), which is the optimal closure energy for which the closure and nonclosure NMEs overlap. The dotted lines (all colors) represent closure NMEs and the solid lines (all colors) represent nonclosure NMEs. Also, black lines (dotted and solid) represent SRC-none case, whereas, the red, blue, and green lines (dotted and solid) represent NMEs for Miller-Spencer, CD-Bonn, and AV18 type SRC, respectively.

parametrizations, whereas, the optimal closure energy is about 2.7 MeV for GT-type NMEs. The optimal closure energy for tensor-type NMEs is around 0 MeV. Since the GT component dominates the total NMEs, therefore, optimal closure energy for total NME is about 2.9 MeV which is similar to GT-type NMEs.

In the end, by determining the optimal closure energy, it is easy to obtain the nonclosure NMEs using the closure approximation with fewer computational resources. We showed the results of closure NMEs along with nonclosure NMEs in Table II with closure energy $\langle E \rangle = 3$ MeV which is near the optimal value for total NMEs. Hence, closure and nonclosure NMEs in Table II are very similar. Also, as discussed in the previous subsection, the use of $\langle E \rangle = 3$ MeV in the closure method reproduced the nonclosure NME using the

closure approach across all cutoff number of states for each spin-parity of the intermediate nucleus ^{124}Sb .

E. NMEs for $2\nu\beta\beta$ decay and its dependence on the cutoff number of states and excitation energy of 1^+ spin-parity of ^{124}Sb

For completeness and concluding our investigation, we finally calculate the NME and half-life for two-neutrino double beta ($2\nu\beta\beta$) decay of ^{124}Sn and examine the dependence of NMEs for $2\nu\beta\beta$ decay of ^{124}Sn on the cutoff number of states and excitation energy of the virtual intermediate nucleus ^{124}Sb . The $2\nu\beta\beta$ decay process is similar to $0\nu\beta\beta$ decay, except that $2\nu\beta\beta$ is a lepton number-conserving decay where two antineutrinos appear in the final state, along with two electrons. The $2\nu\beta\beta$ decay of ^{124}Sn to ^{124}Te , along with two

electrons and two antineutrinos, is expressed as

$${}^{124}\text{Sn} \rightarrow {}^{124}\text{Te} + e^- + e^- + \bar{\nu}_e + \bar{\nu}_e. \quad (13)$$

The half-life of the $2\nu\beta\beta$ decay of the 0^+ ground state to the 0^+ ground state transition is given by [54–56]

$$[T_{1/2}^{2\nu}]^{-1} = G^{2\nu} g_A^4 |m_e c^2 M_{GT}^{2\nu}|^2, \quad (14)$$

where $G^{2\nu}$ is the phase-space factor [54]. In this case, only the Gamow-Teller type NME ($M_{GT}^{2\nu}$) are relevant, and it can be written as [54]

$$M_{GT}^{2\nu} = \sum_{k, E_k^* \leq E_c} \frac{\langle f | |\sigma \tau_2^-| | k \rangle \langle k | |\sigma \tau_1^-| | i \rangle}{E_k^* + E_0}, \quad (15)$$

where τ^- is the isospin lowering operator. In this study, $|i\rangle$ represents the 0^+ ground state of the parent nucleus ${}^{124}\text{Sn}$, $|f\rangle$ represents the 0^+ ground state of the grand-daughter nucleus ${}^{124}\text{Te}$, and $|k\rangle$ represents the 1^+ states of the intermediate nucleus ${}^{124}\text{Sb}$. The E_k^* and E_c are the excitation energy and cutoff excitation energy of the 1^+ states of ${}^{124}\text{Sb}$, respectively. We can also use the cutoff number of states (N_c) for 1^+ spin-parity of ${}^{124}\text{Sb}$ instead of E_c to calculate NME for $2\nu\beta\beta$ decay. The constant E_0 is given by $E_0 = Q_{\beta\beta}(0^+)/2 + \Delta M$. Here, $Q_{\beta\beta}(0^+)$ is the Q value corresponding to the $\beta\beta$ decay of ${}^{124}\text{Sn}$, and ΔM is the mass difference between the ${}^{124}\text{Sb}$ and ${}^{124}\text{Sn}$ isotopes. For the calculation, the bare value of $g_A = 1.27$ is used.

The significance of quenching in the Gamow-Teller operator ($\sigma\tau^-$) cannot be overstated when aiming for congruence between theoretical $2\nu\beta\beta$ NME results and experimental data. This quenching factor (q_f) modifies the Gamow-Teller operator ($\sigma\tau^-$) to $q_f\sigma\tau^-$. In Ref. [9], a quenching factor of 0.74 was employed for the $2\nu\beta\beta$ NME calculation of ${}^{124}\text{Sn}$ within the nuclear shell model, using the SVD Hamiltonian. Alternatively, when employing the GCN5082 Hamiltonian, a value of $q_f = 0.57$ was deemed more suitable for the $2\nu\beta\beta$ NME computations of ${}^{128}\text{Te}$ and ${}^{130}\text{Te}$, while $q_f = 0.45$ was found appropriate for ${}^{136}\text{Xe}$ in Ref. [57]. Recent investigations, as reported in Ref. [58], considered quenching factors of $q_f = 0.48$ and $q_f = 0.42$ for the study of the two-neutrino double electron capture ($2\nu\text{ECEC}$) transition of ${}^{124}\text{Xe}$, employing the GCN5082 Hamiltonian in nuclear shell model. It is evident that a specific quenching factor for ${}^{124}\text{Sn}$ is not yet established. Since the present study employs the same GCN5082 Hamiltonian, a quenching factor of $q_f = 0.4$, a value consistent with earlier studies in the $A \sim 124$ mass region, is used for computing the NME for the $2\nu\beta\beta$ decay of ${}^{124}\text{Sn}$.

The calculated NME for $2\nu\beta\beta$ decay of ${}^{124}\text{Sn}$, including the first 200 states of the virtual intermediate nucleus ${}^{124}\text{Sb}$ with $J^\pi = 1^+$, is 0.014. The corresponding $T_{1/2}^{2\nu}({}^{124}\text{Sn})$ is predicted to be 14.14×10^{21} yr. Table IV lists the calculated NME and $T_{1/2}^{2\nu}({}^{124}\text{Sn})$ as well as NMEs from some of the recent calculations.

Figure 5 illustrates the variation of the NMEs for $2\nu\beta\beta$ decay, computed using the total GCN5082 interaction, with the cutoff number of 1^+ states (N_c) considered for the virtual intermediate nucleus ${}^{124}\text{Sb}$. Our calculations with the

TABLE IV. The calculated NME and half-life for $2\nu\beta\beta$ decay of ${}^{124}\text{Sn}$ using nuclear shell model. Phase-space factor $G^{2\nu} = 5.31 \times 10^{-19}$ (yr^{-1}) is used which is taken from Ref. [9]. The half-lives for other references are recalculated with the quoted NME and g_A of those references with the phase space factor of this study.

Nuclear model	Reference	g_A	NME ($M_{GT}^{2\nu}$ (MeV^{-1}))	$T_{1/2}^{2\nu}$ (yr)
ISM	Current study	1.270	0.014	14.14×10^{21}
ISM	Ref. [9]	1.270	0.042	1.6×10^{21}
ISM	Ref. [51]	1.250	0.101	0.29×10^{21}
QRPA	Ref. [52]	1.254	0.193	0.078×10^{21}
QRPA	Ref. [53]	1.250	0.110	0.24×10^{21}
QRPA	Ref. [7]	1.000	0.200	0.18×10^{21}

available computational facility were able to account for the effects of the first 200 1^+ states of ${}^{124}\text{Sb}$ and the full convergence was not observed for the $2\nu\beta\beta$ NME of ${}^{124}\text{Sn}$. It should be mentioned that for higher shell-model dimensional nuclei like ${}^{124}\text{Sn}$, it is imperative to use a different convergence technique as opposed to the direct diagonalization method employed in the present study. Some possible alternatives are the pioneering strength function approach (see Ref. [59]), or the approach employed in Ref. [60]. Various methodologies and the NME convergence challenges in the context of $2\nu\beta\beta$ decay are discussed in Ref. [61]

In Fig. 6, we demonstrate the dependence of NMEs for $2\nu\beta\beta$ decay on the cutoff excitation energy (E_c) of 1^+ states in the virtual intermediate nucleus ${}^{124}\text{Sb}$. Our computations, which incorporated the effects of the first 200 1^+ states of ${}^{124}\text{Sb}$ using the KSHELL software, were able to capture excitation energies up to about 4 MeV, resulting in computed NMEs as shown in Fig. 6.

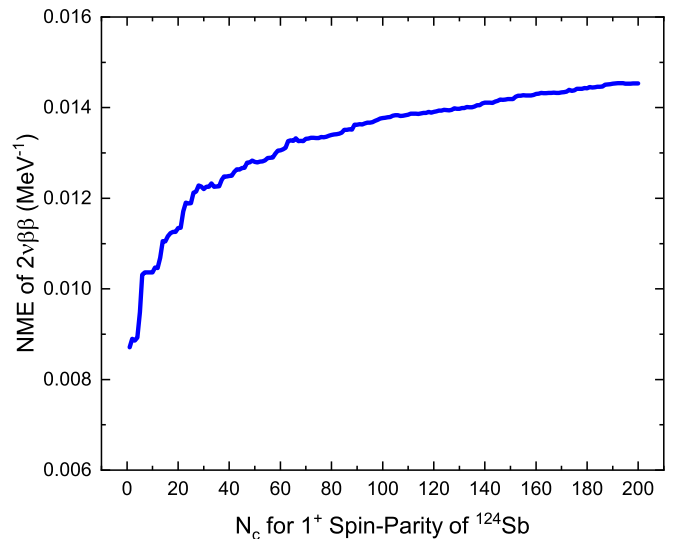


FIG. 5. Variation of the NME for the $2\nu\beta\beta$ decay of ${}^{124}\text{Sn}$ as a function of N_c , the cutoff number of states for 1^+ spin-parity of the virtual intermediate nucleus ${}^{124}\text{Sb}$. The N_c is a dimensionless quantity.

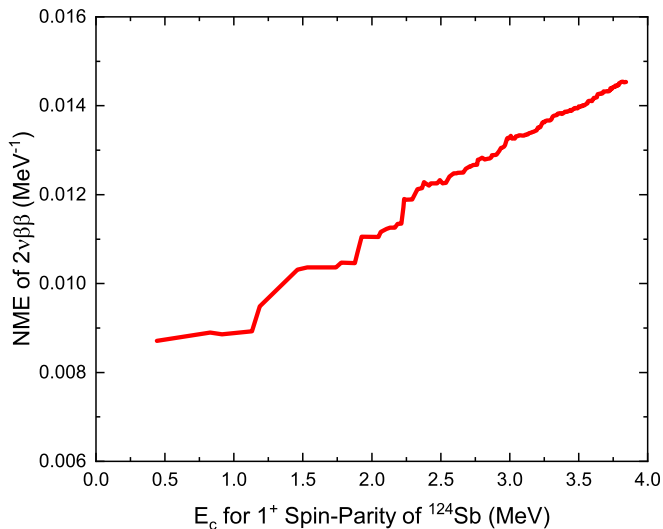


FIG. 6. Variation of the NME for the $2\nu\beta\beta$ decay of ^{124}Sn as a function of E_c , the cutoff excitation energy for 1^+ spin-parity of the virtual intermediate nucleus ^{124}Sb .

V. SUMMARY AND CONCLUSIONS

The nuclear structure study of ^{124}Sn is of great significance as it is an important candidate for $0\nu\beta\beta$, and hence of interest to the double β decay community in India. The NMEs are a crucial input in extracting the $\langle m_{\beta\beta} \rangle$ from the measured $T_{1/2}^{0\nu}$.

In the present work, the NMEs for the $0\nu\beta\beta$ decay of ^{124}Sn (the light neutrino-exchange mechanism) are calculated within the nuclear shell model framework employing the nonclosure approach with improved reliability, by explicitly including the excitation energy for 100 states of each spin-parity of the intermediate nucleus ^{124}Sb .

It is observed that the present method resulted in a 10% variation in NMEs, as compared to the recent closure approach calculations with a nuclear shell model with different input Hamiltonian and closure energy. The difference may arise either due to the choice of the input Hamiltonian or the choice of closure energy in the earlier studies.

The present calculation of NME predicts a lower $T_{1/2}^{0\nu}$ limit as 7.49×10^{26} yr, to achieve a sensitivity of $\langle m_{\beta\beta} \rangle \leq 50$ meV, which is needed to probe the Majorana nature of neutrino in the inverted mass ordering region.

Furthermore, we have analyzed the dependence of NMEs on the spin-parity of intermediate states in ^{124}Sb , as well as that of coupled protons and neutrons. The contributions of each spin-parity of the intermediate states were all positive for GT-type NMEs and negative for Fermi-type NMEs. For coupled spin-parity of protons and neutrons, the 0^+ and 2^+ contributed the most in all NMEs. The effect of the number of intermediate states on the saturation of NMEs has also been investigated. Full convergence was not achieved when 100 intermediate states were taken into account for each spin-parity of ^{124}Sb in the calculation of NMEs for $0\nu\beta\beta$ decay in ^{124}Sn .

It may be pointed out that the choice of the closure energy is arbitrary without the knowledge of the nonclosure NMEs. Hence, the optimal closure energy for which closure and nonclosure NMEs overlap has been calculated and found to be about 3 MeV for $0\nu\beta\beta$ decay of ^{124}Sn . This value successfully reproduced the nonclosure NME using the closure approach across all cutoff number of states for each spin-parity of the intermediate nucleus ^{124}Sb . This is one of the important findings of the present study. The calculated optimal closure energy can be used in future calculations of the closure approach, thereby eliminating the complexity of calculating a large number of intermediate states.

Additionally, the results of variation of NMEs for $2\nu\beta\beta$ decay of ^{124}Sn with the cutoff excitation energy and number of states of the intermediate nucleus ^{124}Sb , including 200 states for the 1^+ spin-parity of ^{124}Sb , are also presented. However, a complete convergence for the $2\nu\beta\beta$ NME in ^{124}Sn is not achieved.

In the future, it will be interesting to explore how the nonclosure approach can affect the NMEs for other beyond standard model mechanisms, such as the left-right symmetric mechanisms.

ACKNOWLEDGMENTS

We gratefully acknowledge the support provided by the Board of Research in Nuclear Sciences (BRNS), Government of India, through project Grant No. 58/14/08/2020-BRNS/37085. Y.I. is thankful to the Tokyo Institute of Technology for generously allowing to use their high-performance computing facility to perform some nuclear state calculations using the KSHELL code.

- [1] M. Agostini, G. Benato, J. A. Detwiler, J. Menéndez, and F. Vissani, Toward the discovery of matter creation with neutrinoless $\beta\beta$ decay, *Rev. Mod. Phys.* **95**, 025002 (2023).
- [2] M. J. Dolinski, A. W. P. Poon, and W. Rodejohann, Neutrinoless double-beta decay: Status and prospects, *Annu. Rev. Nucl. Part. Sci.* **69**, 219 (2019).
- [3] J. D. Vergados, H. Ejiri, and F. Šimkovic, Neutrinoless double beta decay and neutrino mass, *Int. J. Mod. Phys. E* **25**, 1630007 (2016).

- [4] J. Engel and J. Menéndez, Status and future of nuclear matrix elements for neutrinoless double-beta decay: A review, *Rep. Prog. Phys.* **80**, 046301 (2017).
- [5] S. Abe *et al.* (KamLAND-Zen Collaboration), Search for the Majorana nature of neutrinos in the inverted mass ordering region with KamLAND-Zen, *Phys. Rev. Lett.* **130**, 051801 (2023).
- [6] M. Aker *et al.* (KATRIN Collaboration), Direct neutrino-mass measurement with sub-electronvolt sensitivity, *Nat. Phys.* **18**, 160 (2022).

- [7] F. Šimkovic, V. Rodin, A. Faessler, and P. Vogel, $0\nu\beta\beta$ and $2\nu\beta\beta$ nuclear matrix elements, quasiparticle random-phase approximation, and isospin symmetry restoration, *Phys. Rev. C* **87**, 045501 (2013).
- [8] E. Caurier, J. Menéndez, F. Nowacki, and A. Poves, Influence of pairing on the nuclear matrix elements of the neutrinoless $\beta\beta$ decays, *Phys. Rev. Lett.* **100**, 052503 (2008).
- [9] M. Horoi and A. Neacsu, Shell model predictions for ^{124}Sn double- β decay, *Phys. Rev. C* **93**, 024308 (2016).
- [10] B. A. Brown, M. Horoi, and R. A. Sen'kov, Nuclear structure aspects of neutrinoless double- β decay, *Phys. Rev. Lett.* **113**, 262501 (2014).
- [11] Y. Iwata, N. Shimizu, T. Otsuka, Y. Utsuno, J. Menéndez, M. Honma, and T. Abe, Large-scale shell-model analysis of the neutrinoless $\beta\beta$ decay of ^{48}Ca , *Phys. Rev. Lett.* **116**, 112502 (2016).
- [12] J. Barea and F. Iachello, Neutrinoless double- β decay in the microscopic interacting boson model, *Phys. Rev. C* **79**, 044301 (2009).
- [13] J. Barea, J. Kotila, and F. Iachello, Limits on neutrino masses from neutrinoless double- β decay, *Phys. Rev. Lett.* **109**, 042501 (2012).
- [14] T. R. Rodríguez and G. Martínez-Pinedo, Energy density functional study of nuclear matrix elements for neutrinoless $\beta\beta$ decay, *Phys. Rev. Lett.* **105**, 252503 (2010).
- [15] L. S. Song, J. M. Yao, P. Ring, and J. Meng, Relativistic description of nuclear matrix elements in neutrinoless double- β decay, *Phys. Rev. C* **90**, 054309 (2014).
- [16] J. M. Yao, L. S. Song, K. Hagino, P. Ring, and J. Meng, Systematic study of nuclear matrix elements in neutrinoless double- β decay with a beyond-mean-field covariant density functional theory, *Phys. Rev. C* **91**, 024316 (2015).
- [17] P. K. Rath, R. Chandra, K. Chaturvedi, P. K. Raina, and J. G. Hirsch, Uncertainties in nuclear transition matrix elements for neutrinoless $\beta\beta$ decay within the projected-Hartree-Fock-Bogoliubov model, *Phys. Rev. C* **82**, 064310 (2010).
- [18] S. Pastore, J. Carlson, V. Cirigliano, W. Dekens, E. Mereghetti, and R. B. Wiringa, Neutrinoless double- β decay matrix elements in light nuclei, *Phys. Rev. C* **97**, 014606 (2018).
- [19] X. B. Wang, A. Hayes, J. Carlson, G. Dong, E. Mereghetti, S. Pastore, and R. B. Wiringa, Comparison between variational monte carlo and shell model calculations of neutrinoless double beta decay matrix elements in light nuclei, *Phys. Lett. B* **798**, 134974 (2019).
- [20] V. Cirigliano, W. Dekens, J. de Vries, M. L. Graesser, E. Mereghetti, S. Pastore, M. Piarulli, U. van Kolck, and R. B. Wiringa, Renormalized approach to neutrinoless double- β decay, *Phys. Rev. C* **100**, 055504 (2019).
- [21] V. Nanal, Search for neutrinoless double beta decay in ^{124}Sn , *EPJ Web Conf.* **66**, 08005 (2014).
- [22] N. K. Mondal, India-based neutrino observatory (INO), *Euro. Phys. J. Plus* **127**, 106 (2012).
- [23] A. Neacsu and M. Horoi, Shell model studies of competing mechanisms to the neutrinoless double-beta decay in ^{124}Sn , ^{130}Te , and ^{136}Xe , *Adv. High Energy Phys.* **2016**, 1903767 (2016).
- [24] C. F. Jiao, M. Horoi, and A. Neacsu, Neutrinoless double- β decay of ^{124}Sn , ^{130}Te , and ^{136}Xe in the Hamiltonian-based generator-coordinate method, *Phys. Rev. C* **98**, 064324 (2018).
- [25] M. Horoi and A. Neacsu, Shell model study of using an effective field theory for disentangling several contributions to neutrinoless double- β decay, *Phys. Rev. C* **98**, 035502 (2018).
- [26] F. Ahmed and M. Horoi, Interference effects for $0\nu\beta\beta$ decay in the left-right symmetric model, *Phys. Rev. C* **101**, 035504 (2020).
- [27] J. Menendez, A. Poves, E. Caurier, and F. Nowacki, Disassembling the nuclear matrix elements of the neutrinoless beta beta decay, *Nucl. Phys. A* **818**, 139 (2009).
- [28] R. A. Sen'kov and M. Horoi, Neutrinoless double- β decay of ^{48}Ca in the shell model: Closure versus nonclosure approximation, *Phys. Rev. C* **88**, 064312 (2013).
- [29] R. A. Sen'kov and M. Horoi, Shell-model calculation of neutrinoless double- β decay of ^{76}Ge , *Phys. Rev. C* **93**, 044334 (2016).
- [30] R. A. Sen'kov and M. Horoi, Accurate shell-model nuclear matrix elements for neutrinoless double- β decay, *Phys. Rev. C* **90**, 051301(R) (2014).
- [31] R. A. Sen'kov, M. Horoi, and B. A. Brown, Neutrinoless double- β decay of ^{82}Se in the shell model: Beyond the closure approximation, *Phys. Rev. C* **89**, 054304 (2014).
- [32] S. Sarkar, P. Kumar, K. Jha, and P. K. Raina, Sensitivity of nuclear matrix elements of $0\nu\beta\beta$ of ^{48}Ca to different components of the two-nucleon interaction, *Phys. Rev. C* **101**, 014307 (2020).
- [33] S. Sarkar, Y. Iwata, and P. K. Raina, Nuclear matrix elements for the λ mechanism of $0\nu\beta\beta$ decay of ^{48}Ca in the nuclear shell-model: Closure versus nonclosure approach, *Phys. Rev. C* **102**, 034317 (2020).
- [34] F. Šimkovic, G. Pantis, J. D. Vergados, and A. Faessler, Additional nucleon current contributions to neutrinoless double β decay, *Phys. Rev. C* **60**, 055502 (1999).
- [35] J. Kotila and F. Iachello, Phase-space factors for double- β decay, *Phys. Rev. C* **85**, 034316 (2012).
- [36] F. Šimkovic, A. Faessler, H. Mütter, V. Rodin, and M. Stauf, $0\nu\beta\beta$ -decay nuclear matrix elements with self-consistent short-range correlations, *Phys. Rev. C* **79**, 055501 (2009).
- [37] M. Horoi and S. Stoica, Shell model analysis of the neutrinoless double- β decay of ^{48}Ca , *Phys. Rev. C* **81**, 024321 (2010).
- [38] P. Vogel, Nuclear structure and double beta decay, *J. Phys. G: Nucl. Part. Phys.* **39**, 124002 (2012).
- [39] S. Sarkar and Y. Iwata, Effect of spin-dependent short-range correlations on nuclear matrix elements for neutrinoless double beta decay of ^{48}Ca , *Universe* **9**, 444 (2023).
- [40] M. Kortelainen, O. Civitarese, J. Suhonen, and J. Toivanen, Short-range correlations and neutrinoless double beta decay, *Phys. Lett. B* **647**, 128 (2007).
- [41] M. Kortelainen and J. Suhonen, Improved short-range correlations and $0\nu\beta\beta$ nuclear matrix elements of ^{76}Ge and ^{82}Se , *Phys. Rev. C* **75**, 051303(R) (2007).
- [42] D. Štefánik, R. Dvornický, F. Šimkovic, and P. Vogel, Reexamining the light neutrino exchange mechanism of the $0\nu\beta\beta$ decay with left- and right-handed leptonic and hadronic currents, *Phys. Rev. C* **92**, 055502 (2015).
- [43] J. Barea, J. Kotila, and F. Iachello, $0\nu\beta\beta$ and $2\nu\beta\beta$ nuclear matrix elements in the interacting boson model with isospin restoration, *Phys. Rev. C* **91**, 034304 (2015).
- [44] J. Hyvärinen and J. Suhonen, Nuclear matrix elements for $0\nu\beta\beta$ decays with light or heavy Majorana-neutrino exchange, *Phys. Rev. C* **91**, 024613 (2015).
- [45] A. Faessler, M. González, S. Kovalenko, and F. Šimkovic, Arbitrary mass Majorana neutrinos in neutrinoless double beta decay, *Phys. Rev. D* **90**, 096010 (2014).

- [46] N. Shimizu, T. Mizusaki, Y. Utsuno, and Y. Tsunoda, Thick-restart block Lanczos method for large-scale shell-model calculations, *Comput. Phys. Commun.* **244**, 372 (2019).
- [47] E. Caurier, F. Nowacki, A. Poves, and K. Sieja, Collectivity in the light xenon isotopes: A shell model study, *Phys. Rev. C* **82**, 064304 (2010).
- [48] K. Harigaya, M. Ibe, and T. T. Yanagida, Seesaw mechanism with Occam's razor, *Phys. Rev. D* **86**, 013002 (2012).
- [49] T. Asaka, Y. Heo, and T. Yoshida, Lepton flavor model with modular A_4 symmetry in large volume limit, *Phys. Lett. B* **811**, 135956 (2020).
- [50] K. Asai, Predictions for the neutrino parameters in the minimal model extended by linear combination of $U(1)_{L_e-L_\mu}$, $U(1)_{L_\mu-L_\tau}$ and $U(1)_{B-L}$ gauge symmetries, *Eur. Phys. J. C* **80**, 76 (2020).
- [51] E. Caurier, F. Nowacki, A. Poves, and J. Retamosa, Shell model study of the neutrinoless double beta decays, *Nucl. Phys. A* **654**, 973c (1999).
- [52] J. Suhonen and O. Civitarese, Weak-interaction and nuclear-structure aspects of nuclear double beta decay, *Phys. Rep.* **300**, 123 (1998).
- [53] J. Suhonen, On the double-beta decays of ^{70}Zn , ^{86}Kr , ^{94}Zr , ^{104}Ru , ^{110}Pd and ^{124}Sn , *Nucl. Phys. A* **864**, 63 (2011).
- [54] M. Doi, T. Kotani, and E. Takasugi, Double beta decay and Majorana neutrino, *Prog. Theor. Phys. Suppl.* **83**, 1 (1985).
- [55] T. Tomoda, Double beta decay, *Rep. Prog. Phys.* **54**, 53 (1991).
- [56] W. C. Haxton and G. J. Stephenson, Double beta decay, *Prog. Part. Nucl. Phys.* **12**, 409 (1984).
- [57] E. Caurier, F. Nowacki, and A. Poves, Shell model description of the $\beta\beta$ decay of ^{136}Xe , *Phys. Lett. B* **711**, 62 (2012).
- [58] E. A. Coello Pérez, J. Menéndez, and A. Schwenk, Two-neutrino double electron capture on ^{124}Xe based on an effective theory and the nuclear shell model, *Phys. Lett. B* **797**, 134885 (2019).
- [59] E. Caurier, A. P. Zuker, and A. Poves, A Full $0\hbar\omega$ description of the $2\nu\beta\beta$ decay of ^{48}Ca , *Phys. Lett. B* **252**, 13 (1990).
- [60] J. Engel, W. C. Haxton, and P. Vogel, Effective summation over intermediate states in double-beta decay, *Phys. Rev. C* **46**, R2153(R) (1992).
- [61] M. Horoi, Double beta decay: A shell model approach, *Physics* **4**, 1135 (2022).